High-Temperature Spectrometer for Thermal Protection System Radiation Measurements

S. M. White*

NASA Ames Research Center, Moffett Field, California 94035

DOI: 10.2514/1.45222

To better characterize the response of thermal protection system materials to predicted near-infrared shock layer radiation, a new experimental system was developed to extend the measurement range of radiation transport parameters to high-temperature environments and relatively high-radiation fluxes. A portable research-grade spectrometer was coupled with fiber optics in order to operate in a variety of harsh operating environments. Experimental results are presented from tests performed at the solar tower, which provided broadband nonpulsed visible and infrared radiation at relatively high-flux levels. Data from three low-density porous refractory fibrous materials are presented, including two shuttle tile materials (fibrous refractory composite insulation and Lockheed International) and one carbon fiber material. The results showed that thin 1 and 2 mm specimens of the ceramic tile materials acted as robust high-temperature gray filters in the near infrared, whereas thicker tile specimens (and 1 mm and thicker porous carbon fiber matrix samples tested) absorbed the incident radiation strongly and exhibited only thermal radiation spectral profiles.

Nomenclature

a_M = mean absorption coefficient
a_P = Planck mean absorption coefficient
a_R = Rosseland mean absorption coefficient
d_i = physical thickness of sample i, cm
$e_{\lambda b}$ = hemispherical spectral blackbody emissive power, $W/cm^2 \mu$
k = mean extinction coefficient, including scattering and absorption, $1/cm$
k_λ = spectral extinction coefficient, including scattering and absorption, $1/cm$
q_{rad} = radiative flux, W/cm^2
$q_{\lambda,z}$ = spectral radiative flux in the z direction, W/cm^2
r_λ = spectral reference beam for a given incident flux, counts
$s_{i\lambda}$ = spectral signal measured for test sample i for a given incident flux, counts
t = time exposure or duration, s
z = distance in the z or incident direction, cm
α_λ = spectral absorptance
ρ_λ = spectral reflectance
σ = Stefan–Boltzmann constant, $W/cm^2 \cdot K^4$
τ_λ = spectral transmittance
∇T = temperature gradient, K/m

I. Introduction

FUTURE crewed spacecraft for lunar or planetary missions may use larger, more massive, and faster blunt-body entry vehicles, which will experience substantially increased shock layer heating [1] upon atmospheric entry. The predicted atmospheric entry heating includes high levels of both convective as well as radiative heating in narrow bands dictated by shock layer thermochemistry (at much higher radiation levels than those experienced by previously crewed Earth return vehicles). A high-density heat shield material successfully protected Galileo against the extreme combined radiation and convection heating environment it experienced at Jupiter in 2003. However, such a high-density thermal protection system (TPS) is not an efficient or viable option for many missions, and NASA is developing designs with low-density porous TPS materials for many upcoming demanding missions. Low-density porous TPS materials include reusable insulation as well as low-density ablative TPS. Reusable materials do not degrade as a result of a design heating cycle, whereas ablators exploit blowing and absorb energy by sacrificing mass through thermochemical reactions, including organic resin pyrolysis. Low-density porous TPS handle convective heating very well, but the response of most spacecraft TPS materials to high levels of radiation is unknown. Low-density porous materials could potentially transmit significant levels of radiation either directly or by scattering, allowing repeated opportunities for in-depth absorption at each interface with in-depth heating.

The low- to mid-density TPS materials used by NASA's current space program include both passive and ablative porous composite materials, which exhibit variable material properties as functions of temperature and pressure. There remains significant uncertainty about the interaction of shock layer radiation with low-density and mid-density porous materials over the temperature range of interest, during which the chemical composition and the local density of the ablative material change considerably via pyrolysis and charring. The potential for material degradation or failure due to spectral transmission and in-depth absorption of significant levels of radiation energy cannot be ignored.

Ideally, the spacecraft TPS materials for a high-radiation atmospheric entry would be perfectly opaque high-emittance or high-reflectance materials, which would efficiently absorb and reemit or reflect most or all the incident radiation at the surface without transmitting a significant fraction of the incident radiation and without suffering any significant in-depth absorption of the radiative energy.

When the materials perform either as surface absorbers or as optically thick media in all wavelengths of concern, straightforward models can be used. In the simplest case for modeling and performance, the material would act as a surface absorber, totally opaque to all incident radiation and modeled using conventional boundary conditions. If the material is optically thick, then transmission and in-depth absorption of radiation drops rapidly as radiation diffuses through the material in a manner analogous to diffusion due to thermal conductivity through a solid material. Radiation diffusion through an optically thick medium is modeled using an increased effective conductivity by including the radiative conductivity. In an ablator, the char layer and pyrolysis zone extend to characteristic temperature thresholds for given conditions. In the case that radiation

diffusion increases the total effective conductivity, radiation energy transport could result in higher in-depth temperatures and thicker char layers in comparison with pure convection cases, as limited previous work may have indicated [2–5]. Comparable radiation and convection tests could not be run under identical pressures but, in the relatively impermeable materials of interest, the pressure dependence of the thermal conductivity appears to be too weak to account for key observations. In the worst case, semitransparency and in-depth absorption could lead to higher in-depth and bondline temperatures and possible material failure.

Radiation transport follows entirely different rules from convection or conduction heat transfer [6–8] , and so it is necessary to model it separately and to make dedicated measurements to characterize and quantify radiation transport through the materials of interest. Modeling would require simultaneously solving Maxwell's equations with the energy transport equations and rigorously modeling the material geometry and radiation transport. The radiation transport properties at the wavelengths and operational temperatures of interest for the candidate low- to mid-density ablators, however, are not well characterized. Unless the thermal protection material used on a vehicle absorbs or reflects most significant shock layer radiant energy at its surface (or it is optically thick), then rigorous modeling is challenging, and in-depth transmission and absorption could occur at susceptible wavelengths and result in excessive in-depth heating.

Therefore, several TPS materials' spectral transmittance and reflectance were measured to assess the relevant radiation transport properties for current and future use in order to more confidently include radiation transport in thermal models.

The room-temperature and moderate-temperature spectral transmittance and reflectance measurements, which can be accurately made in a laboratory, are insufficient to confidently predict how the material will handle substantial levels of radiation at operational temperatures during pyrolysis and at predicted radiation fluxes. Previous data on high-density materials are limited and cannot be extrapolated well to the lower density materials or to the radiation fluxes at the wavelengths and levels of current interest to NASA. For these reasons, a flexible, reasonably portable new spectrometry test setup was needed to extend the measurement range of radiation transport parameters to more realistic operational temperatures and to allow measurements to be made using relatively high-radiation flux from several different radiant sources. This paper describes the experimental setup, testing, and modifications to develop the capability to better characterize the response of porous refractory fiber materials to near-infrared (NIR) radiation, with data from three materials.

II.   Background

Two historical flight vehicles included successful experiments designed to make direct measurements of the shock layer radiation: the 1965 Fire II vehicle and the 1967 Apollo 4 vehicle. Test data from these flights, in addition to ground test data, have been used to numerically simulate shock layer radiation with regard to both spectral distribution and intensity. Fire II used a passively insulating TPS, and the Apollo 4 vehicle used an ablative TPS. The radiation intensity at the TPS surface was measured through a quartz window. This approach produced unique data on shock layer radiation required for the intended missions. These experiments still provide key data for shock layer radiation code calibration to a vehicle surface, but they do not provide information about the TPS material's response to radiation. These experiments and the computational fluid dynamics (CFD) analysis for the new trajectories provided the basis for the relevant wavelength and intensity ranges used for testing in this work. Extensive analyses, based on state-of-the-art CFD tools with modern radiation codes, predicted that shock layer heating to the spacecraft would include a significant radiative heating component over a range of wavelengths [1]. The heating environments predicted for Earth entry for such a vehicle allow the consideration of low- to mid-density materials as reliable and mass-efficient candidate thermal protection materials.

III.   Modeling

An extensive body of literature, including excellent reviews, exists on the modeling of radiation, including refractory fibers and other open porosity materials [6–11]. Modeling approaches range from complex numerical models (starting from first principles using Maxwell's equations) through Mie scattering approaches to engineering correlations as the complexity of the material's behavior or the urgency increases. It represents a substantial challenge to start from first principles to numerically model the interaction of radiation with and between the many randomly oriented fibers, particles, and porous media during heating, pyrolysis, and charring (as appropriate to the material). Unfortunately, neither appropriate temperature- and pressure-dependent material properties, nor sufficient time and budget, were available for this approach, and extensive experimental measurements would still be required for code validation. Instead, an engineering approach was followed to evaluate the response to significant levels of NIR radiation of passive TPS materials to provide a baseline and approach for analysis of more complex ablative materials.

Figure 1 illustrates the transport of radiation at different zones in a charring and pyrolyzing ablative material, with a control volume shown by dashed lines around the pyrolysis zone. In contrast, a passive material does not develop zones of distinct chemistry but can be divided into regions according to the temperature gradient and the composition and optical property gradients developed during heating. The incident radiation, reflection, and emission are shown at the top surface of the control volume, and transmission of the incident radiation and emission from the hot char are shown as radiation inputs to the control volume. Energy outputs from the control volume are shown as the transmitted fractions of the incident radiation and incident emission, as well as thermal emission from the control volume. The test setup was designed to accommodate specimens machined, as in Fig. 1.

Rigorous modeling of energy transport for unrestricted cases with radiation would require simultaneously solving Maxwell's equations with the energy transport equations with complete knowledge of geometry, radiation transport properties, etc. Fortunately, two key limiting cases are relevant for TPS. Ideal surface absorbers are modeled with radiation equilibrium boundary conditions and do not require discussion here. The powerful radiation diffusion method [6] decouples radiation from other heat-transfer modes. The radiation diffusion approximation is valid in the case of an optically thick medium when the radiative heat flux through the material is only weakly coupled to the other energy transfer modes. Under these conditions, radiation transport is included as an energy source gradient term similar to conduction in the energy transport equations for thermal modeling:

$$q_{\text{rad}} = \frac{16\sigma T^3}{3a_M} \nabla T \tag{1}$$
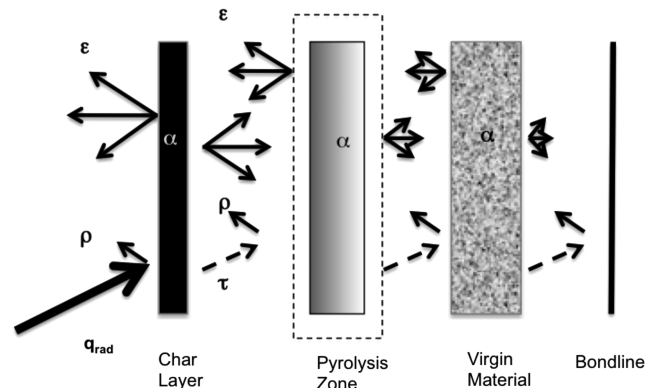

Fig. 1   **Transport of radiation through an ablator in the char layer, the pyrolysis zone, the virgin material, and the bondline.**

The mean absorption coefficient accounts for the absorption and reemission of radiant energy locally within the optically thick material. It is appropriate in heat-transfer computations to integrate the spectral or wavelength-dependent properties to compute a single mean radiative property. The total radiative property for a material of a given thickness (emittance, absorptance, transmittance, or reflectance) is defined as the scaled energy-weighted integrated average of the spectral or wavelength-dependent property. Two widely used mean absorption coefficients defined next are the Rosseland and Planck mean absorption coefficients. The incident energy can fall in a limited wavelength range for shock layer or laser radiation or over a broad wavelength range, such as solar, lamp, or blackbody radiation.

The Rosseland mean absorption coefficient is the integrated spectral absorptance, a function of material conditions, weighted by the local radiation flux, which is a function of both the wavelength and position:

$$a_R = \frac{\int_0^\infty \alpha_\lambda(\lambda, T, p) \cdot \mathrm{d}q_{\lambda,z}}{\int_0^\infty \mathrm{d}q_{\lambda,z}} \qquad (2)$$

The Planck mean absorption coefficient weights the spectral absorptance by the blackbody radiative flux at the local temperature rather than the local radiation flux:

$$a_p = \frac{\int_0^\infty \alpha_\lambda(\lambda, T, p) \cdot e_{\lambda b}(\lambda, T) \cdot \mathrm{d}\lambda}{\sigma \cdot T^4} \qquad (3)$$

These mean absorption coefficients are equivalent under certain conditions (i.e., when the material acts like a gray medium). Ideally, this should be verified with an exact numerical solution of Maxwell's equation for the specific materials, conditions, and geometry. The Planck mean absorption coefficient is significantly easier to incorporate into energy transport modeling than the Rosseland mean coefficient, because it is weighted by the Planck blackbody function in terms of wavelength and the local temperature rather than in terms of the local spectral energy flux, which must be solved for iteratively.

The optical properties transmittance, reflectance, absorptance, and emittance depend on wavelength, temperature, and pressure. The spectral transmittance and reflectance are measured experimentally and are used to calculate the spectral absorptance:

$$\alpha_\lambda + \rho_\lambda + \tau_\lambda = 1 \qquad (4)$$

The test setup described next was used to measure the transmittance of the test materials. Reflectance values were obtained from existing data or measured directly.

The total property after integration over wavelength remains dependent on temperature and chemistry. The angular dependence can be averaged out or limited to a narrow beam for thermal calculations, and the hemispherical or normal value is usually measured for energy transport, as appropriate to the measurement system characteristics or application. Integrating spheres average the energy over all solid angles to directly measure hemispherical properties. Normal values are measured in many direct transmittance and other spectral measurements, including the measurements described here. For isotropic noncrystalline porous composite materials, the random orientation of material components physically averages out the angular dependence to approach the hemispherical values to a large extent.

Optical properties [12] are frequently not available for TPS materials over the range of required conditions and are given the lack of equilibrium and complex geometry of the nonisotropic medium; the most pragmatic engineering approach is to calculate the effective radiation transport properties directly from the experimental data, rather than by numerical modeling. This analytical approach, originally developed for gas, has been extended [6–8] for engineering calculations to gray media (such as soot) and offers valuable insight into this scattering and absorbing porous medium, even with local temperature gradients, nonrandom fiber orientation, and complex composition. The averaged effective value is a useful engineering tool, both as a starting point for more detailed work and for immediate thermal transport estimates.

The Beer–Lambert–Bouguer law states

$$\tau_\lambda = e^{-k_\lambda d_i} = e^{-\int_0^{d_i} k_\lambda(z) \, \mathrm{d}z} \qquad (5)$$

where

$$\tau_\lambda = \frac{s_{i\lambda}}{r_\lambda}$$

The extinction coefficient includes both the scattering and absorption coefficients, which may change with composition, temperature, pressure, and wavelength. In the conventional case of a nonscattering material, the extinction coefficient is independent of thickness. However, for the highly scattering thin tile material test samples used in these measurements, the extinction coefficient exhibited a strong dependence on thickness due to multiple scattering. The extinction coefficient for a fixed thickness was constant for different flux levels, because the scattering geometry was consistent between specimens of the same thickness. The extinction coefficient is, by definition, inversely related to the penetration depth. Direct calculations are made using experimental measurements of the transmitted and forward-scattered signal for a test sample of a given thickness ratioed by the incident radiation, which is the directly measured or scaled reference beam.

IV. Test Setup

A new experimental setup was designed, installed, modified, and calibrated to characterize the spectral radiation transport properties of high-temperature materials subjected to relatively high levels of incident radiation over the NIR wavelength range.

These tests were undertaken to assess the potential risk of material degradation or failure, due to spectral transmission and in-depth absorption, under conditions selected to simulate the NIR shock layer radiation predicted for certain future NASA missions. Because available test setups could not meet NASA's requirements, a new test system was developed to make spectral transmittance measurements on TPS materials over the NIR range of wavelengths predicted to impinge on the TPS surface for certain trajectories. Among the radiation sources investigated, solar concentrators and argon and xenon arc lamps offered the most useful combination of continuous-wave broad-spectrum sources in the infrared with sufficient power for these measurements.

A flexible, portable, and robust research-grade spectrometer and supporting system was developed to adapt to different test environments and requirements. It was designed for use in several different configurations in order to gather infrared transmittance data needed to characterize the relevant radiation transport properties of the candidate TPS materials at radiant flux and temperature conditions that adequately simulate mission requirements.

The test materials were thin samples of high-temperature porous fiber materials machined to thicknesses of 1, 2, 5, and 10 mm to allow comparison over a wide range of test conditions. The test materials had a range of relevant length scales (the sample thickness, pore size, fiber diameter and length), but all these lengths were greater than the 1 μm length scale of the incident NIR wavelength of radiation. The test sample was mounted in a high-temperature ceramic model holder, machined of (Lockheed International) LI-2200 silica fiber space shuttle tile material, for thermal and electrical isolation. A crossflow of clean nitrogen gas was used to blow away decomposition products and to cool the optics while preventing beam blockage and contamination of the optics.

Figure 2 shows a schematic of the experimental setup. The portable spectrometer used was a Princeton Instruments/Acton Spectrapro 2300i 0.3 m focal length, triple-grating spectrometer. The spectrometer's resolution, or minimum resolvable distance between distinct peaks, was 0.1 nm in the visible range, and the dispersion was 2.7 nm/mm. This research-grade instrument has an accuracy of 0.2 nm, and its repeatability is ± 0.05 nm, according to the manufacturer's specifications. The measurement quality was comparable with that of the precision laboratory spectrometers with low-powered lamp sources used for supporting measurements.
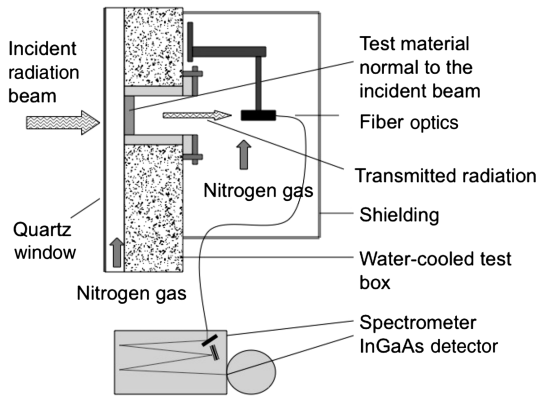
Fig. 2 Schematic of spectral measurement setup, showing the incident and transmitted radiation beam.

A wide range of detectors are available that, when coupled with appropriate gratings, allow measurements over an extensive wavelength range. The NIR wavelength range required for these tests from 0.9 to 1.3 μ falls outside the silicon detector range of 0.3 to 1.1 μ, and so an indium-gallium-arsenide (InGaAs) detector was selected, which is usable over the wavelength range of interest from 0.9 to 1.6 μ. This single-beam dispersive spectrometer can accept single-point or imaging detectors and, during the course of the project, both an InGaAs point detector and a liquid-nitrogen (LN2)-cooled linear array InGaAs detector were used. The point detector proved reliable but required 30 s to scan the wavelength range of interest, during which the materials heated, increased thermal emissions, and/or decomposed. To improve the scan rate, a faster LN2-cooled InGaAs linear array detector was used with a 150 g/mm grating to capture spectra from 0.85 to 1.2 or 1.1 to 1.6 μ in 0.2 s per scan. With the faster scan rate, exposure times could be reduced to separate by detection time the transmission from the thermal radiation.

The spectrometer itself was physically located away from the direct line of sight, up to 12 m from the exposed test materials, in order to protect the spectrometer from the high test temperatures, vibration, interference, and chemical contamination. The test material decomposition products would otherwise condense on the relatively cold optical gratings and mirrors in the equipment. A visible-NIR (VIS-NIR) collimator lens was used to collect the transmitted light from the back face of the sample and couple the light into an optical fiber. The imaged region on the back face was approximately 1 cm in diameter. The collimator lens was positioned 10 cm away from the heated surface. Additional cooling by gas flow was used to keep the lenses below the 250°C maximum operating temperature and further protect against chemical contamination by the decomposition or pyrolysis products of certain test samples during heating, to prevent heating of the adhesives and cladding materials beyond their maximum operating temperature.

The VIS-NIR fibers selected for the experiments were manufactured from anhydrous silica and were rated for use over the 350 to 2200 nm range. The transmittance of these fibers through 1 m of optical fiber range was greater than 99% over the narrow NIR wavelength range of the current test requirements. These fibers are typically used for optical transmission lines that require very high transmittance over kilometers, rather than over the 12 m distance used in these measurements. The fiber ends were standard threaded coaxial connectors and polished flat ends. A refocusing lens could be used to limit the input area when needed. Optical fibers with polished flat ends were used for preliminary tests with shorter 3 m long fibers of identical composition, which limited the energy throughput to that gathered by the fiber end. These polished flat fiber ends accept radiation from a cone of light of about 25 deg (full angle). The fiber end used for input to the spectrometer was a polished flat end at the inlet slit.

To calculate the radiative properties, a reference-beam measurement is required. Different spectrometer designs [13] follow different strategies to acquire and use a reference beam. A dual-beam instrument sends the split-off reference beam through a different, unimpeded path. Single-beam instruments, such as the one employed here, need a separate reference-beam measurement (typically made before the test measurement), which can be used in the software to calculate the absorptance, emittance, or transmittance before the data are displayed or recorded. Alternatively, raw measurements are made of the reference beam and the transmitted or reflected signal and ratioed manually in a postprocessing step. Because of scaling issues, the latter approach was taken.

Because of the high radiative flux of the incident beam relative to the flux transmitted through the samples, reference-beam measurements were acquired using filters or with reduced detector gains and integration times selected to prevent saturation of the InGaAs detector. Preventing saturation was critical, because the recommended procedure to prevent spurious readings after saturation is to allow the detector to warm up to room temperature, then cool it again to operational temperature (100 K), but this process takes several hours and would wreak havoc with the test schedule. The reference-beam measurements were scaled up for direct comparison with the transmitted beam measurements, obtained without filters or at higher detector gains or longer integration times, while tracking the response for nonlinearity.

V. Test Configuration

Several radiation sources were evaluated to provide sufficiently high levels of continuous, rather than pulsed, broadband NIR radiation to irradiate the test materials. Preliminary tests were run at NASA Ames with lower-powered spectrometers. Scaled-up high-power preliminary tests were run at both Sandia National Laboratory and at Oak Ridge National Laboratory to investigate potential high-flux continuous broadband radiation to irradiate sufficiently large areas for this material testing, without pulsing, at the required flux levels and to shake down the entire system. The tests were configured differently for these facilities (due to the differences in geometry, environment, and control), incorporating or excluding reflective filters. This paper describes tests performed at Sandia at the solar tower, also known as the National Solar Thermal Test Facility.

At the solar tower, the test radiative flux level and exposure duration are controlled by coordinated movements of solar heliostat reflectors that focus their reflected beams on the target where the test material is positioned. Initial tests were performed on top of the tower (with the spectrometer and data acquisition computer) located in the observation room, 12 m from the heated target zone at the focal point of the heliostat field. To include modifications and improvements with triggering and a shutter for improved exposure control, as well as an improved test rig that provided better crossflow of nitrogen gas in order to reduce oxidation, later tests were performed at the 240 level wind-tunnel level in the tower.

Figure 2 shows the incident beam impinging on the test sample with a fraction of the beam transmitted through the material to the fiber optic inlet, where it is in turn transmitted by internal reflections along the fiber to the spectrometer. The test box was designed to minimize stray light and was ventilated from below with nitrogen gas flow with light-trap ventilation plugs. The test material was inserted into a silica fiber insulation model holder mounted in a water-cooled holder facing the incident-reflected beam. The fiber optics and collimator input end were mounted on a breadboard in a nitrogen gas ventilated box. The test box was painted with Krylon black inside and was designed to reduce stray light and to control contamination. The spectrometer and data acquisition system were located out of the direct beam path. This positioning was useful for reducing the strong electrical interference and vibration, for keeping the instruments within a good operating temperature range, and for safety.

Figure 3 shows the solar tower, the heliostat field, and the control tower, as seen from the air above Kirtland Air Force Base.

Figure 4 shows the spectrometer and LN2-cooled InGaAs detector on the table in the foreground, with the test box mounted between cooling lines behind the heliostat target in the background. The lower half of the circular white ceramic test model holder is seen inside the open black-painted optical box mounted at the heliostat target.

Figure 5 shows solar radiation, well documented to cover a broad range, from the American Society for Testing and Materials (ASTM)

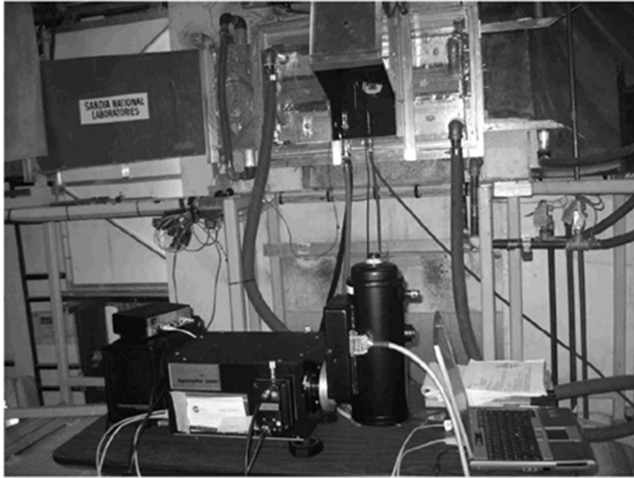Fig. 3   Solar tower at Sandia National Laboratory.

Fig. 4   Spectrometer and test setup.

standard [14] G159-98 direct normal irradiance. Outside the atmosphere, solar radiation is typically modeled as blackbody radiation of a 5777 K perfect blackbody emitter, but atmospheric absorption of energy occurs at characteristic wavelengths due to the presence of water vapor, CO_2, and other gas species.

Figure 6 shows the incident solar radiation measured by the spectrometer, linearly scaled by a fixed value of 0.0139 to compare with the ASTM standard solar spectrum G159-98. The spectrometer, at the time of these measurements, was not yet calibrated against a National Institute of Standards and Technology (NIST)-traceable
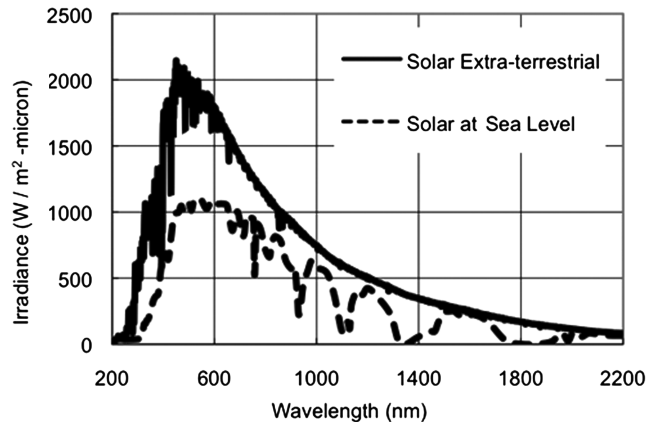
calibrated source to create the response function. Several reflective broadband filters and wire mesh screens were destroyed in attempting reference-beam measurements and, although laser aperture plates showed good potential, they were limited by pinhole camera effects and did not flood the collection optics. Controlling the detector's exposure by limiting the integration time was successful. These measurements were made through an open port, with the incident beam flooding the collimator lens. Thirty heliostats provided 12 W/cm^2 radiation flux for these tests, whereas subsequent runs went to 150 W/cm^2. The results were scaled to give one sun flux for comparison with the standard. Although uncalibrated, these measurements agree well with the standard references for solar radiation at ground level within the 0.9 to 1.5 μ region, in which the instrument is responsive. The high altitude and low humidity at the test site (leading to reduced water absorption), as well as stray light and reflections from the quartz window in front of the test specimen, were also considered as potential complications. Secondary effects were dominated by internal reflections of visible light inside the spectrometer and eliminated using a cold mirror or cutoff filter in later test runs on other materials

The infrared range away from the detector tailoff represents a blackbody fraction of 22.5% of the total solar radiation. Preliminary testing included operating the system with low-power radiant sources in order to test and refine the system without the effects of an absorbing medium in place. Additional tests with a NIST-traceable calibration source were run to rigorously evaluate the system's accuracy.

VI.   Experimental Results

Experimental results are shown next for low flux tests run on selected TPS materials. It was not possible to use the longer 100 ms time directly for the reference measurements, because the detector would have saturated and possibly been damaged, and so these

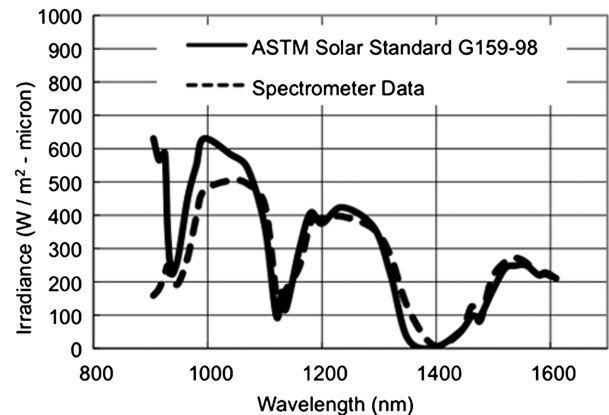Fig. 5   Spectral distribution of infrared solar radiation, from ASTM G159-98.

Fig. 6   Uncalibrated detector measurements of solar spectrum.

measurements were made with a 10 ms integration time. The data shown here were scaled to compensate for the different integration times used for material transmittance measurements (i.e., to give a signal that would have been measured with a 100 ms integration time for use with 100 ms measurements). The spectral transmittance is calculated by ratioing the transmitted spectrum to the scaled incident reference-beam spectrum measured with this equipment at each wavelength. This computation is valid even before the system was calibrated to a traceable standard, because the response function measured by calibration cancels out in the ratio.

The spectra transmitted by both tile materials follows the absorption regions in the solar spectrum, as expected, and show similar secondary effects.

Figure 7 shows the raw signal transmitted, including both direct transmittance and forward scattering, through two thicknesses of the high-temperature silica fibrous insulation LI-2200. The solar power tower used 30 heliostats to give 12 W/cm^2 of radiation flux. The measured transmittance of the 2 mm specimen was an order of magnitude lower than through 1 mm, as expected.

Figure 8 shows the signal transmitted, including the direct and scattered components, through two thicknesses of the high-temperature ceramic fibrous insulation (fibrous refractory composite insulation) FRCI-12. The test conditions were the same as previously shown, with 30 heliostats used to provide 12 W/cm^2 of concentrated solar radiation flux. The measured transmittance through 2 mm was, as expected, significantly lower than through the 1 mm thickness. The overall apparent transmission for FRCI-12 is much higher than for (Lockheed International) LI-2200, mainly due to the fact that the density of FRCI-12 is approximately 55% of LI-2200, with significantly less solid absorbing and scattering material in the beam path. In addition, LI-2200 is composed of silica of a given fiber diameter,
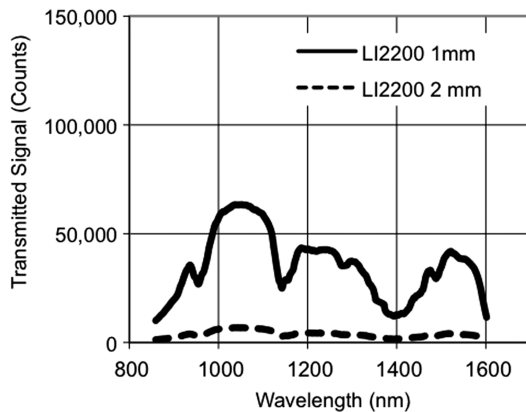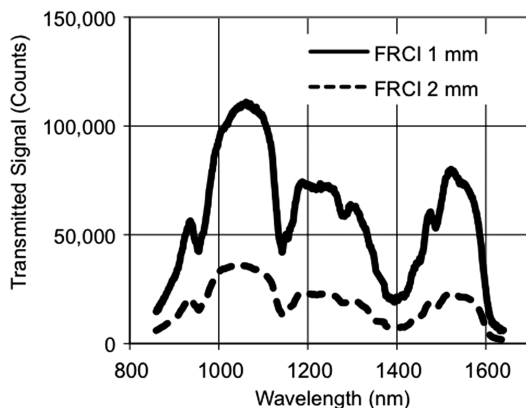
whereas FRCI-12 has a range of fiber diameters and more complex material composition.

Figure 9 shows the signal representing transmitted or emitted energy measured during tests on LI-2200 and FRCI-12 for two thicknesses using 12 W/cm^2 exposures during durations of 20 s. The transmitted energy signal measured did not change during the exposure. Because the signal dropped immediately at the cessation of heating, this is transmitted energy, as opposed to blackbody or thermal radiation. This is consistent with room-temperature laboratory transmission measurements. The extinction coefficient computed from Eq. (5) is not independent of thickness due to scattering effects, as further discussed next. At this flux and at higher fluxes not shown, the spectral transmittance of LI-2200 and FRCI-12 are reasonably independent of the incident NIR wavelength; that is, the thin tile specimens act like useful gray high-temperature filters in this NIR waveband.

Figure 10 shows the peak infrared energy measured at the back face of two Fiber Materials, Inc. carbon fiber form (CFF) models after 5 s of exposure to 12 W/cm^2 flux of concentrated solar energy. Unlike the immediate signal transmittance measured in the thin tile samples, during the first few seconds of exposure, only a negligible signal was measured at the back face of the efficiently absorbing carbonaceous CFF material. Below the detector tailoff at 1600 nm, the peak value increased monotonically from zero to the value shown at 5 s. At 5 s, the run was aborted to prevent the charge-coupled device (CCD) detector from saturating. CFF has an average density of 0.19 g/cm^3. The estimated bulk temperature increased to roughly 600 K for the 1 mm specimen and to 450 K for the 2 mm-thick specimen. Previous runs with an electronically cooled InGaAs point detector yielded the low signal shown at wavelengths below 1150 nm. Therefore, for efficiency, the wavelength range from 850 to 1150 nm was not repeated with the CCD or for 1 mm thickness. As the carbon material heats up, it emits an increasing profile that, adjusting for the nonlinear detector tailoff at 1600 nm, follows a classical temperature-dependent blackbody spectrum. The absorbing CFF response stands in contrast to the predominantly scattering, nonabsorbing materials FRCI-12 and LI-2200, which instantly transmitted the incident spectrum.

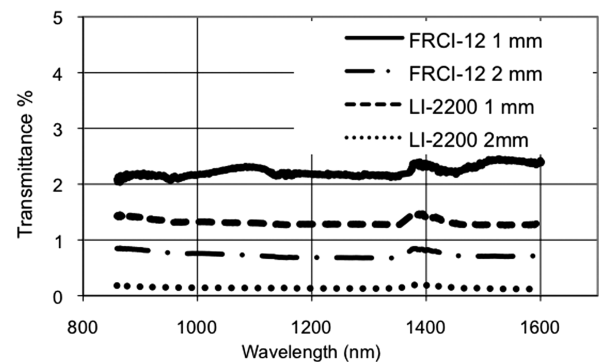
Fig. 7   Uncalibrated raw spectral measurements through two thicknesses of LI-2200.

Fig. 8   Uncalibrated spectral transmission measurements through two thicknesses of FRCI-12.

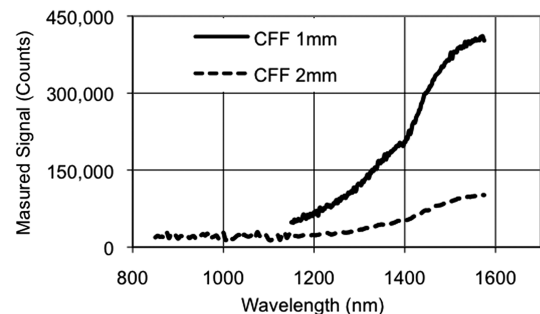**Fig. 9   Transmittance during exposure of FRCI-12 and LI-2200.**

Fig. 10   back face signal measurements after heating of 1- and 2-mm-thick CFF.

VII. Discussion

A predictable difference was seen between lab bench spectrometer measurements with integrating spheres to include all forward-scattering components and these new normal high-flux measurements. Using the NASA Ames Perkin–Elmer Lambda 9 UV/VIS/NIR laboratory spectrometer, 1 mm specimens of FRCI-12 and LI-2200 showed 3 and 2% transmittance, respectively, and 2 mm samples of FRCI-12 and LI-2200 showed 1.5 and 0.2% transmission, respectively. These higher values result from the integrating sphere collecting all forward-scattering components. The tile materials remained at room temperature during these exposures, in contrast to the absorbing CFF, which heated substantially during testing, and so a first-order estimate of the spectral absorptance can be calculated for energy balance purposes with Eq. (5), using the measured room-temperature NIR reflectance with the transmittance measured here at higher flux. Measurements made with a conventional low-powered laboratory Perkin–Elmer UV/VIR/NIR spectrometer gave NIR reflectances of 75% for FRCI-12 and 85% for LI-2200. This gives dimensionless NIR absorptance values for 2-mm-thick specimens of FRCI-12 of 0.03 and of LI-2200 of 0.02. When CFF was exposed to a low flux of incident radiation, the transmittance of a 1-mm-thick CFF specimen was negligible from 0.5 to 18 μ at room temperature, as in the solar data.

Data from sufficiently high-flux solar test runs on thicker specimens of the tile materials LI-2200 and FRCI-12 showed no immediate transmission but instead, after heating, showed blackbodylike profiles similar to the CFF data. This is consistent with the much greater number of repeated scattering and absorbing interactions at the fiber surfaces in thicker specimens. Even at 12 W/cm^2 flux, a weak thermal blackbody profile was measured though 5 mm of FRCI-12. Test runs at higher fluxes were distributed like thermal emission.

Comparing the subset of data from only the 2 mm specimen runs, the data consistently followed the Beer–Lambert–Bouguer law at all fluxes up to 150 W/cm^2. The 1-mm-thick samples showed less consistent behavior, which is believed to be due to the thin sample inhomogeneity. The average overall effective radiation NIR extinction coefficient was calculated as 25 cm^{-1} for FRCI-12 and 33 cm^{-1} for the much higher density LI-2200 for the NIR spectral range of 0.85 to 1.6 μ, based on the 2 mm test data. The density-scaled mass coefficients, related to the cross sections, were 128 cm^2/g for FRCI-12 and 93 cm^2/g for the pure silica LI-2200 material.

Because the radiation diffusion approximation is considered valid [6] for engineering calculations for optical thickness, the extinction coefficient times the thickness greater than 2; this indicates that the radiation diffusion approximation is valid for these materials for all practical thicknesses on the centimeter scale and larger.

Estimating the ratio of the Rosseland radiative conductivity to the thermal conductivity gives a value of 25% at 400 and 600 K for FRCI-12 and LI-2200, respectively, and 50% at 600 and 850 K for FRCI-12 and LI-2200, respectively.

In contrast, the CFF showed absorption-dominated behavior. Physically, a ray of incident radiation undergoes repeated absorption and reemission at the many fiber interfaces within the carbon fiber medium before emerging at the material's back face, in contrast to mainly scattering by the predominantly nonabsorbing fibers, as in the tile materials tested. At each interface with the highly absorbing carbon fibers, the radiation is absorbed and reemitted with an altered wavelength distribution governed by temperature-dependent blackbody radiation. This behavior is analogous to the behavior in high-temperature soot [7] that, however, has a smaller size scale. The internal geometry of CFF is also analogous to blackbody cavities, as well as to drilled holes or partly closed cavities, which approach blackbody cavity behavior when their aspect ratios approach appropriate limits [6]. The end result of the incident radiation's interaction with the carbon fiber matrix is to convert the wavelength distribution of the incident solar energy from the visible and near infrared farther into the infrared.

To directly measure the data through the predicted maximum in the infrared, increasing the spectral region covered by the instrumentation would account for more of the spectral energy. The efficiently absorbing behavior of carbon dominates transport in the carbon fiber matrix, producing a thermal radiation profile through rapid absorption and reemission. The reflectance of amorphous carbon-based materials is intrinsically low, and high-temperature carbon properties are available in the literature. With data obtained with the present instrumentation, it is not possible to rigorously calculate a spectral penetration depth for CFF, but using the integrated data from 1 mm thickness gives an estimated extinction coefficient reasonably consistent with other carbon data [8,12] of 77 cm^{-1}, giving a mass coefficient of 400 cm^2/g. Computing the ratio of the Rosseland radiative conductivity to the thermal conductivity gives a value of 25% at 1850 K and 50% at 2600 K.

VIII. Conclusions

This paper describes a new experimental setup to measure TPS porous material transmittance at relatively high fluxes, and the results presented demonstrate this experimental design has the flexibility to adapt a research-grade spectrometer to measure radiative transport properties under a variety of harsh conditions beyond a well-controlled laboratory environment. Improvements in several areas were identified and incorporated.

Data from three low-density fibrous refractory TPS materials are shown. The two tile materials, FRCI-12 and LI-2200, scattered without absorption and acted as well behaved and effective spectrally gray NIR transmitters of radiation at 1 and 2 mm thicknesses; that is, they performed well as stable, gray, high-temperature NIR filters. This has useful applications, because the commercially available filters tested did not survive the direct exposure under these test conditions. In contrast, even 1 mm of the low-density CFF shifted the wavelength distribution of the incident radiation into the infrared, rapidly absorbing and reemitting the incident energy as thermal radiation. Extinction coefficients were calculated for these open porosity materials, indicating that the radiation diffusion approximation is valid for material thicknesses greater than the centimeter scale. In these cases, it is both pragmatic and appropriate to decouple the radiative from the convective heating mode in energy transport modeling, using the powerful radiation diffusion approximation to compute an effective thermal diffusivity.

References

[1] Olynick, D., Henline, W., Hartung-Chambers, L., and Candler, G., "Comparison of Coupled Radiative Flow Solutions with Project Fire 2 Flight Data," *Journal of Thermophysics and Heat Transfer*, Vol. 9, No. 4, 1995, pp. 586–594.
doi:10.2514/3.712

[2] White, S., Skokova, K., and Laub, B., "Char Development in Atmospheric Entry Simulation Tests of Low-Density Ablators," *53rd JANNAF Propulsion Meeting*, Baltimore, MD, Dec. 2005.

[3] Laub, B., and White, S., "Arcjet Screening of Candidate Ablative Thermal Protection Materials for Mars Science Laboratory," *Journal of Spacecraft and Rockets*, Vol. 43, No. 2, 2006, pp. 367–373.
doi:10.2514/1.19218

[4] Congdon, W. M., "Thermal Radiation Characteristics of the Mars Heat Shield Material for Flight Data Analysis," 31st AIAA Thermophysics Conference, AIAA Paper 1996-1888, June 1996.

[5] Congdon, W. M., Curry, D. M., and Collins, T. J., "Response Modeling of Lightweight Charring Ablators and Thermal Radiation Testing Results," 39th AIAA/ASME/SAE/ASEE Joint Propulsion Conference and Exhibit, AIAA Paper 2003-4657, July 2003.

[6] Siegel, R., and Howell, J. R., *Thermal Radiation Heat Transfer*, 2nd ed., McGraw–Hill, New York, 1981, Chaps. 8, 15, 19.

[7] Eckert, E. R. G., Tien, C. L., and Edwards, D. K., "Radiation," *Handbook of Heat Transfer Fundamentals*, 2nd ed., edited by W. M. Rohsenow, J. P. Harnett, and E. N. Ganik, McGraw–Hill, New York, 1985, Chap. 14.

[8] Howell, J. R., and Menguk, M. P., *Handbook of Heat Transfer*, 3rd ed., edited by W. M. Rohsenow, J. P. Harnett, and Y. I. Cho, McGraw–Hill, New York, 1998, Chap. 7.

[9] Cunnington, G., Lee, S. C., and White, S. M., "Radiative Properties of Fiber-Reinforced Aerogel: Theory vs Experiment," *Journal of Thermophysics and Heat Transfer*, Vol. 12, No. 1, 1998, pp. 17–22.
      doi:10.2514/2.6318

[10] Kumar, S., and White, S., "Dependent Scattering Properties of Woven Fibrous Insulations for Normal Incidence," *Journal of Heat Transfer*, Vol. 117, No. 1, Feb. 1995, pp. 160–167.
      doi:10.1115/1.2822297

[11] Lee, S. C., White, S. M., and Grzesik, J., "Effective Radiative Properties of a Fibrous Composite Containing Spherical Particles," *Journal of*

Thermophysics and Heat Transfer, Vol. 8, No. 3, 1994, pp. 400–405.
      doi:10.2514/3.556

[12] Musikant, S., *Optical Materials*, Optical Engineering, Vol. 6, Marcel Dekker, New York, 1985, Chaps. 1, 8.

[13] Coates, J., "A Review of Sampling Methods for Infrared Spectroscopy," *Applied Spectroscopy: A Compact Reference for Practitioners*, edited by J. Workman, Jr., and A. Springsteen, Academic Press, San Diego, CA, 1998, pp. 50–91, 493–496.

[14] "Standard Tables for References Solar Spectral Irradiance at Air Mass 1.5: Direct Normal and Hemispherical for a 37 deg Tilted Surface," American Society for Testing and Materials Standard G159-98 West Conshohocken, PA, 1999.
      doi:10.1520/G0159-98

G. Palmer
Associate Editor